

Mechanisms and Site Selectivity of (Het)Ar–X Oxidative Addition to Pd(o) Are Controlled by Frontier Molecular Orbital Symmetry

Jingru Lu,[†] Nathan D. Schley,[‡] Irina Paci,^{†*} and David C. Leitch^{†*}

[†]Department of Chemistry, University of Victoria, 3800 Finnerty Rd., Victoria, BC V8P 5C2, Canada.

[‡]Department of Chemistry, Vanderbilt University, Nashville, Tennessee 37235, United States.

KEYWORDS: cross-coupling, oxidative addition, palladium catalysis, site-selectivity, quantitative modeling

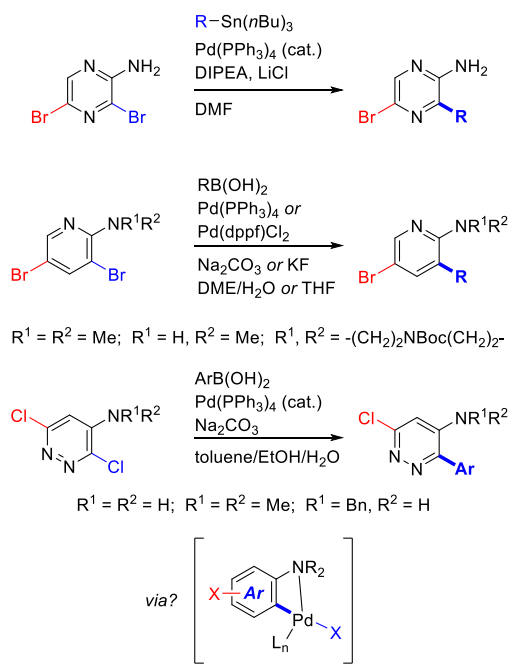
ABSTRACT: We report how the reaction mechanism and site-selectivity of 2-halopyridine oxidative addition to L₂Pd(o) are both controlled by frontier molecular orbital symmetry. Comparing oxidative addition rates for pairs of 2-chloro-3-EDG-pyridines / 2-chloro-5-EDG-pyridines (EDG = electron-donating group: NH₂, OMe and F) to Pd(PCy₃)₂ reveals the 3-EDG isomers undergo oxidative addition ~100 times faster than their 5-EDG counterparts ($\Delta\Delta G^{\ddagger}_{\text{OA}} = 10.4\text{--}11.6 \text{ kJ mol}^{-1}$). Experimental and computational mechanistic studies reveal that the LUMO symmetries of the substrates control the oxidative addition mechanism. For the 3-EDG derivatives, high LUMO orbital coefficients at the reactive C₂ position, and antibonding LUMO symmetry through the C₂=N bond of the pyridine lead to a nucleophilic displacement oxidative addition mechanism. Conversely, the LUMO of the 5-EDG derivatives has a node through the C₅–C₂ plane, leading to minimal orbital contribution at the reactive carbon. The higher energy LUMO+1 has substantial density at C₂, but minimal orbital density at the nitrogen. This leads to 5-EDG substrates undergoing a 3-centered insertion oxidative addition mechanism. These orbital symmetry effects also control site-selectivity for multihalogenated pyridines, which we investigate for both electron-donating and electron-withdrawing substituents. Incorporating simple frontier orbital based molecular descriptors to a quantitative multivariate linear model for oxidative addition leads to improved prediction accuracy for both relative rates and site-selectivity of substituted 2-halopyridine oxidative addition to L₂Pd(o).

INTRODUCTION

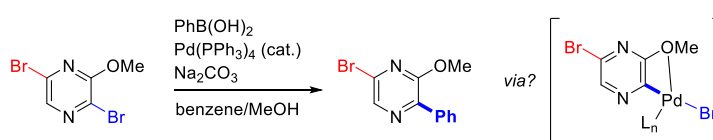
Palladium-catalyzed cross-coupling continues to be a powerful synthetic method to form new bonds between two molecular fragments. Its wide application in pharmaceutical and chemical industries makes it among the most important reactions in modern organic synthesis.^{1,2} Oxidative addition is often the rate and/or selectivity determining step of the catalytic cycle, and understanding its mechanism is crucial for optimizing reaction conditions and improving site-selectivity in synthesis cases.³ The mechanisms of Ar–X oxidative addition to Pd(o) have been extensively studied among different types of organic (pseudo)halides and palladium complexes.^{4–15} The specific oxidative addition mechanism, and its corresponding influence on site-selectivity, is determined by a number of interrelated factors, including the structure of the electrophile, the identity of the (pseudo)halide, the coordination number of the Pd(o) species, the structure of the ancillary ligands, the reaction solvent, and the presence of additives.^{16–23}

One common strategy to control site-selectivity in metal-catalyzed reactions is the incorporation of a coordinating directing group.^{18,20,24–26} Pre-coordination of the substrate to these groups places the catalytic center proximal to a specific reactive site, leading to selective functionalization. While many well-characterized examples of directing group coordination are reported, especially for C–H functionalization reactions, there are many cases where pre-coordination is invoked to explain site-selectivity with no direct evidence. This includes several cases of site-selective cross-coupling reactions where oxidative addition is directed to a site proximal to Lewis basic functional groups (Figure 1). For example, amino groups direct coupling to *ortho* C–X sites in multiply halogenated heterocycles; coordination of Pd to the amino group is used to explain these effects, but no direct evidence of this coordination is reported (Figure 1A).^{27–30} Similarly, ether groups direct coupling to *ortho* sites, which is again rationalized with coordination to the oxygen (Figure 1B).³¹

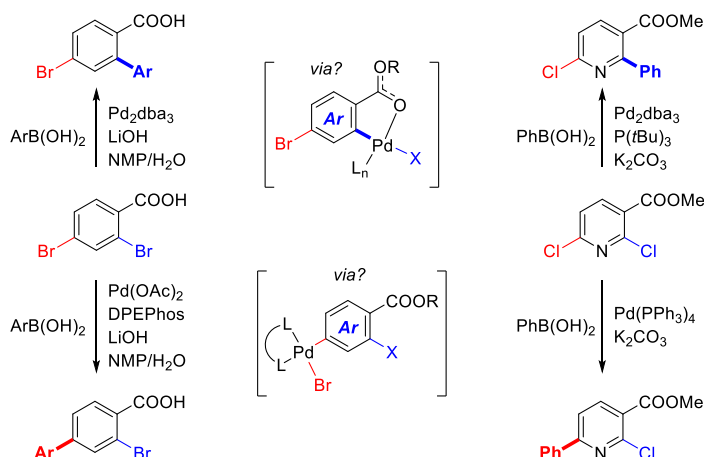
A Amine-directed oxidative addition



B Ether-directed oxidative addition



C Carboxylate/Ester-directed oxidative addition



D This work: substituents affect frontier molecular orbital symmetry

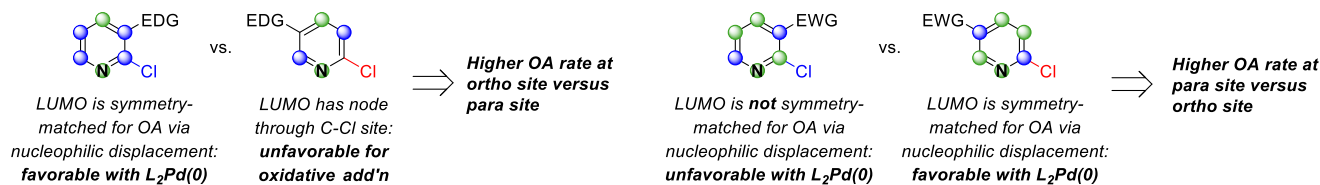


Figure 1. Examples of substituent directing effects in Pd-catalyzed cross-coupling reactions. **A)** Amine directing groups in Stille and Suzuki coupling with halogenated heterocycles, with putative proposed intermediate involving Pd–N coordination. **B)** Methoxy-directed Suzuki coupling, with putative proposed intermediate. **C)** Carboxylate and ester directing groups in Suzuki cross-coupling, with divergent site-selectivity dependent on ligand identity. **D)** Frontier molecular orbital symmetry dictates oxidative addition mechanistic features, and explains site-selectivity with $L_2Pd(o)$ catalysts (EDG = electron-donating group; EWG = electron-withdrawing group).

However, in many cases this coordination is likely unfavorable. Anilines and aryl ethers are poor ligands for Pd(o) due to their high donor atom electronegativities, and delocalization of the lone-pair into π -symmetry molecular orbitals. Furthermore, the putative Pd(II) intermediates would be five coordinate if oxidative addition proceeds from an $L_2Pd(o)$ species (such as with smaller and/or bidentate phosphines^{32,33}). The use of carboxylate and ester directing groups highlights these Pd speciation effects (Figure 1C),^{34,35} where high site-selectivity for the C–X position *ortho* to the directing group requires no added phosphine (for carboxylates) or a bulky phosphine to favor oxidative addition from LPd(o) ($P(tBu)_3$ for esters). If bidentate (e.g. DPEPhos) or simple (e.g. PPh_3) phosphines are used, leading to $L_2Pd(o)$ as the relevant species, the opposite site-selectivity is observed.

Herein, we offer an alternative explanation for substituent directing effects in Pd-catalyzed cross-couplings that

proceed *via* $L_2Pd(o)$ intermediates. Rather than directly coordinating to the 14-electron Pd center, substituents instead influence the LUMO symmetry of the substrate (Figure 1D). Changes to these orbital symmetries lead to differences in the oxidative addition mechanism, affecting both the rate and site-selectivity. Accordingly, relative reactivity and site-selectivity predictions can be made by incorporating substrate LUMO descriptors into a multivariate linear model for oxidative addition to $L_2Pd(o)$.

RESULTS AND DISCUSSION

Electron-donating substituents on 2-chloropyridines. We recently developed a structure-reactivity relationship for (Het)Ar–X oxidative addition to $L_2Pd(o)$ that is able to quantitatively predict relative reactivity and conventional site-selectivity for a variety of substrates.³⁶ This model uses simple, mechanistically-relevant molecular descriptors to account for electronic and steric effects,

as well as (*pseudo*)halide identity. These include average molecular electrostatic potential (*ESP*) at specific atoms in the substrate,^{37–41} substituent *A*-values to account for sterics,⁴² and the intrinsic bond strength index (*IBSI*)⁴³ for the C–X bond strength. The resulting quantitative reactivity and selectivity predictions are accurate not only within the training/test dataset, but also in external case studies with complex molecules. Importantly for the present work, the model parameters do not directly include any molecular orbital features.

While interrogating the few clear outliers to our model's predictions as evidence for possible mechanistic changes, we noted an apparent systematic discrepancy between predicted and experimental oxidative addition relative rates (given as $\Delta\Delta G^{\ddagger}_{\text{OA}}$) between three related substrate pairs: 2-chloro-3/5-amino-pyridine, 2-chloro-3/5-methoxypyridine and 2-chloro-3/5-fluoropyridine (Figure 2). These substrate pairings have very similar predicted oxidative addition rates (based on very similar *ESP* values at the key atoms), regardless of whether the electron-donating group (EDG) is in the 3- or 5-position (predicted $\Delta\Delta G^{\ddagger}_{\text{OA}} = 0.3$ – 3.4 kJ mol⁻¹). However, the difference in experimental oxidative addition rates is substantial (observed $\Delta\Delta G^{\ddagger}_{\text{OA}} = 10.4$ – 11.6 kJ mol⁻¹). In each case, the 3-EDG substrates are faster than predicted, while the 5-EDG substrates are slower than predicted.

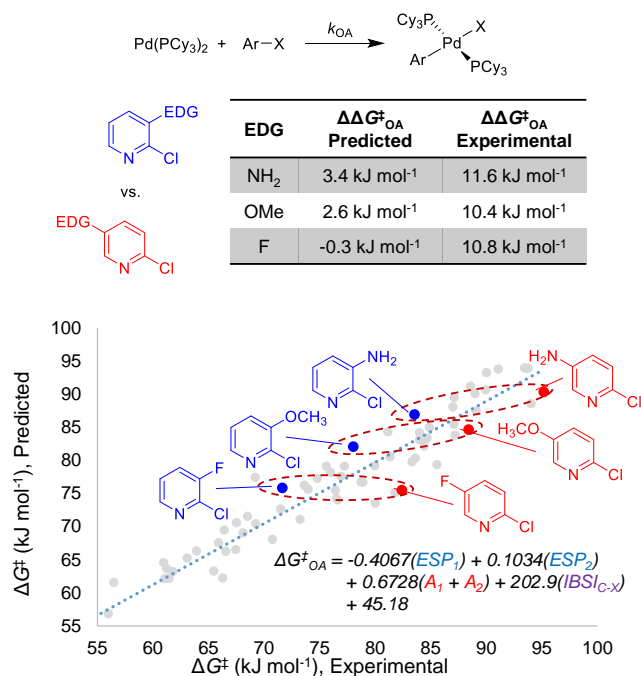


Figure 2. Relative rates of oxidative addition for 2-chloro-3/5-EDG-pyridines to Pd(PCy₃)₂, showing a clear and systematic discrepancy between predicted and actual rate differences. ($\Delta\Delta G^{\ddagger}_{\text{OA}} = \Delta G^{\ddagger}_{\text{OA}}$ (2-Cl-5-EDG-py) – $\Delta G^{\ddagger}_{\text{OA}}$ (2-Cl-3-EDG-py)). Data and model from ref. 36.

As discussed in the Introduction and Figure 1, one possibility is that the 3-amino and 3-methoxy groups coordinate to Pd(o) to accelerate the oxidative addition rate at the *ortho* C–Cl bond; however, this is extremely unlikely for the 3-fluoro case. We also used DFT calculations in an attempt

to locate putative intermediate Pd(o) structures and Pd(II) oxidative addition products that exhibit coordination to the 3-amino or 3-methoxy groups; however, no stable structures could be located. Finally, while directing group coordination would explain the faster-than-predicted rates observed for 3-EDG substrates, it does not explain the slower-than-predicted rates for the 5-EDG analogues. All of these factors prompted us to formulate alternative hypotheses for the discrepancies between the predicted and experimental rates.

Recently, Neufeldt and coworkers reported that site-selectivity in Pd-catalyzed cross-coupling of 2,4-dihalogenated pyridines can be predicted by the *HOMO* symmetry of the Pd(o) species undergoing oxidative addition.¹⁵ Specifically, a change in Pd-based *HOMO* symmetry from π in 14-electron L₂Pd(o) species (bent geometry) to σ in 12-electron LPd(o) species can override conventional site-selectivity, favoring oxidative addition at the 4-position of the pyridine rather than the 2-position.

Inspired by this work, we hypothesized that orbital symmetry – which is not accounted for in our predictive model – could be a valid explanation for the rate divergence between substrate pairings in Figure 2. Specifically, we reasoned that changes to the *LUMO* symmetry of the substrate could result in different oxidative addition mechanisms. In related recent work from our lab on building predictive models for nucleophilic aromatic substitution (S_NAr) reactions, we encountered several cases where the electrophile *LUMO* / *LUMO*+1 symmetries determine the site-selectivity of substitution with dihalopyridines.⁴⁴ To assess this hypothesis, we have conducted a combined computational and experimental study of oxidative addition rate and site-selectivity for substituted halopyridines to L₂Pd(o), using Pd(PCy₃)₂ as an exemplar.⁴⁵ In a concurrent and complementary study, Neufeldt and co-workers further establish the interplay between Pd speciation, ligand identity, and orbital symmetry in determining the mechanism of oxidative addition for unsubstituted phenyl-X and pyridyl-X substrates (X = F, Cl, Br, I, OTf).⁴⁶

We first computationally analyzed the oxidative addition mechanisms/transition states for the series 2-chloro-3/4/5-EDG-pyridine (EDG = NH₂, OMe, F); the case of the –NH₂ derivatives is shown in Figure 3 (see the Supporting Information, Table S7 and Figures S65–75 for details on all substrates). These results are consistent with experimental observations, with oxidative addition TS[‡] energies in the order 3-NH₂ < 4-NH₂ < 5-NH₂. Furthermore, the calculated $\Delta\Delta E^{\ddagger}_{\text{OA}}$ of 13.3 kJ mol⁻¹ between the 3-NH₂ and 5-NH₂ transition states is quantitatively consistent with experiment ($\Delta\Delta G^{\ddagger}_{\text{OA}} = 11.6$ kJ mol⁻¹). Importantly, these calculations reveal that two distinct mechanisms operate depending on the substituent location.

For the 3-amino derivative, we can locate a discrete intermediate (INT_{3-NH₂}) where the Pd(o) center coordinates to the C=N bond of the pyridine. The subsequent oxidative addition TS[‡] is characteristic of a nucleophilic displacement mechanism:⁴⁴ first, there is a short Pd–N (2.29 Å) length, a long Pd–Cl (3.10 Å) length, and a relatively obtuse

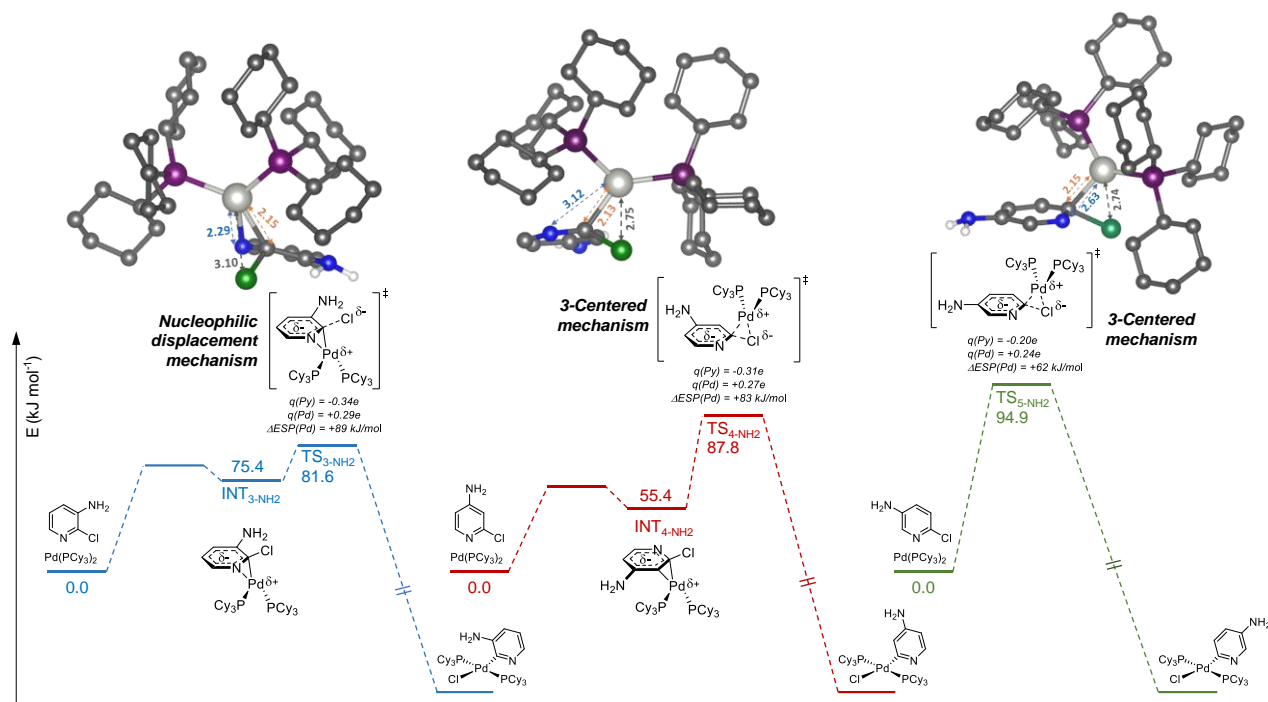


Figure 3. Simplified reaction coordinate diagrams for the oxidative addition of 2-chloro-3/4/5-NH₂-pyridine to Pd(PCy₃)₂, showing a change in mechanism from nucleophilic displacement (3-NH₂ substrate, blue coordinate) to 3-centered insertion (4- and 5-NH₂ substrates, red and green coordinates). Transition state geometries were optimized with CPCM(THF) at RI BP86 def2-SVP def2/J level with D3BJ dispersion for all atoms except for Pd, for which a def2-TZVP basis set was used. Single point energies were calculated at RI-B2PLYP D3 def2-TZVP def2-TZVP/C level with CPCM(THF).

C-Pd-Cl angle (95.4°), consistent with minimal Pd-Cl bonding; second, the TS[‡] has considerable partial negative charge delocalized on the pyridine (-0.34e) as well as partial positive charge at Pd (+0.29e); third, there is a large increase in ESP at the Pd center from Pd(PCy₃)₂ to the transition state ($\Delta ESP = +89$ kJ mol⁻¹). These characteristics are shared by the oxidative addition TS[‡] structures for the 3-OMe and 3-F derivatives (Figures S68, S71, and S74-75).

In contrast, the 4-NH₂ and 5-NH₂ pyridine derivatives undergo a more traditional 3-centered oxidative addition mechanism, with higher $\Delta E_{\text{OA}}^{\ddagger}$ values than the 3-NH₂ oxidative addition TS[‡]. For 4-NH₂, we located a pre-coordination intermediate with Pd(0) coordinated to a C=C π -bond rather than the C=N bond; this is also the case for the 4-OMe and 4-F derivatives. For the 5-NH₂ and 5-OMe derivatives, we could not locate stable pre-coordination intermediates along the reaction coordinate, with the Pd(0) bound to either to the C=N bond or C=C π -bond or elsewhere on the pyridine ring; however, we did locate an intermediate for the 5-F derivative, with Pd(0) coordinated to the C=N π -bond.

The structures of the 3-centered transition states have distinct characteristics, including long Pd-N (2.58-3.12 Å) and shorter Pd-Cl (2.74-2.81 Å) distances, more acute C-Pd-Cl angles (81.8-84.6°), and lower partial charges on both the pyridine ring and the Pd center. In general, there is a smaller increase in ESP at Pd between Pd(PCy₃)₂ and these TS[‡] structures relative to the corresponding nucleophilic displacement TS[‡] (e.g. $\Delta ESP = +83$ and +62 kJ mol⁻¹

for the 4-NH₂ and 5-NH₂ TS[‡] structures respectively). All of these features point to a more symmetric, less polarized TS[‡] than for the nucleophilic displacement TS[‡].¹⁴ In all cases, attempts to locate the alternative oxidative addition TS[‡] type (3-centered for 3-EDG substrates, nucleophilic displacement for 4/5-EDG substrates) were not successful.

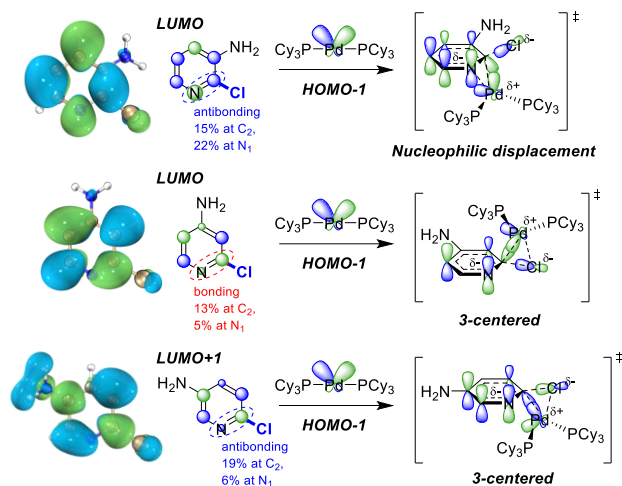


Figure 4. Relevant FMOs of the 2-chloro-3/4/5-amino-pyridines (*LUMO* for 3/4-NH₂ and *LUMO+1* for 5-NH₂) and Pd(PCy₃)₂ (*HOMO-1* in linear geometry; becomes *HOMO* in bent geometry⁴⁷) leading to oxidative addition transition states shown.

This change in oxidative addition mechanism for the 2-chloro-3/4/5-EDG-pyridine systems flows directly from frontier molecular orbital considerations (Figure 4). The 14-electron Pd(PCy₃)₂ has a π -symmetric HOMO-1 orbital, which becomes the HOMO as the P-Pd-P bond is bent away from a linear geometry.⁴⁷ This enables Pd to synergistically bond to the π systems of aromatic substrates, activating them toward oxidative addition. For the substrates, the -NH₂ substituted pyridines are illustrated as a representative case (Figure 4). The LUMO of the 3-NH₂ derivative has a nodal plane cutting through the C₂=N bond, leading to antibonding symmetry between these two atoms, and large LUMO coefficients at both C₂ (15%) and N (22%). These LUMO properties are well-matched with the HOMO-1 of L₂Pd(o), leading to strong bonding between Pd and the C₂=N bond in the π -complex intermediate, further stabilizing the nucleophilic displacement transition state.

For the 4-NH₂ derivative, the LUMO coefficient is 13% at C₂; however, C₂ and N have π -bonding symmetry between the two atoms in the LUMO, which prevents Pd(PCy₃)₂ pre-coordination to the C₂=N bond. Instead, C₂ and C₃ are π -antibonding in the LUMO, making the C₂=C₃ bond the preferred site for Pd(PCy₃)₂ coordination. This is consistent with DFT calculations that reveal just such a C₂=C₃ pre-coordination intermediate for the 4-NH₂ derivative, followed by a 3-centered transition state with the Pd(PCy₃)₂ unit bonded to only the C₂ atom.

For the 5-NH₂ derivative, the LUMO coefficient at C₂ is very small (5%) due to a nodal plane cutting through C₂ and C₅. Such low orbital density at the reactive center indicates that the LUMO is not the relevant frontier orbital involved in the transformation at C₂. In contrast, the LUMO+1 coefficient at C₂ is much higher, accounting for 19% of the orbital density. Visualizing the HOMO of the 3-centered transition state, which is formed from interaction between the bonding orbital of Pd(PCy₃)₂ and antibonding orbital of the substrate, reveals the LUMO+1 is the participating orbital for the 5-NH₂ derivative. As the LUMO+1 is higher in energy, the TS[‡] for the oxidative addition of the 5-NH₂ derivative will also be higher in energy, leading to a slower rate. These characteristics of the frontier orbitals and their connections to the reaction mechanism and reactivity trend (3-EDG > 4-EDG > 5-EDG) are shared by the -OMe and -F groups (see Supporting Information, Figures S68-S75).

To further test this frontier molecular orbital (FMO) based hypothesis, we studied the connection between frontier orbital properties and the oxidative addition rates with three more pairs of 2-chloro-3/5-EDG-pyridines (Figure 5). By analogy, the 3-EDG substrates, with high LUMO coefficients at C₂ and antibonding orbital symmetry at the C₂=N bond, are expected to proceed via the nucleophilic displacement TS[‡]. The 5-EDG substrates, with low LUMO coefficients at C₂, are expected to undergo a higher energy 3-centered pathway. The observed relative rates agree well with this hypothesis, where $\Delta\Delta G^{\ddagger}_{\text{OA}}$ is 8.9 kJ mol⁻¹ for the -O(iPr) pair, and 7.6 kJ mol⁻¹ for the -NHCOMe pair. The -OtBu pair is notable: even with a sterically large group at the C₃ site, the 3-OtBu substrate is still faster than the 5-

OtBu derivative ($\Delta\Delta G^{\ddagger}_{\text{OA}} = 1.9$ kJ mol⁻¹). This is an example where the frontier orbital impact is significant enough to partly override the steric effect, though sterics do cause the 3-OtBu derivative to be slower than the 3-OiPr substrate in an absolute sense. Finally, single crystal XRD characterization of the oxidative addition complex from the 3-NHCOMe derivative confirms no directing group coordination to Pd(II) in the product.

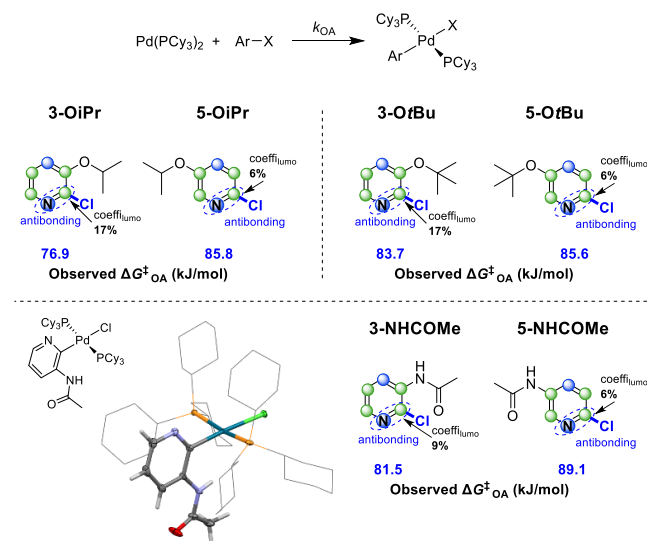


Figure 5. $\Delta\Delta G^{\ddagger}_{\text{OA}}$ values for the oxidative addition of the indicated 2-chloropyridine substrates to Pd(PCy₃)₂, and schematics of the LUMO for each substrate, with 3-EDG derivatives consistently faster than their 5-EDG counterparts. Solid-state molecular structure of the oxidative addition complex formed with 2-chloro-3-acetamidopyridine pictured, confirming no directing group coordination in the product (thermal ellipsoids plotted at 50% probability, cyclohexyl groups plotted as wireframe with no hydrogen atoms for clarity).

Frontier orbital symmetries and site-selectivity. To test if these FMO insights are relevant to site-selectivity predictions, we investigated the oxidative addition reactivity of three sets of dihalogenated heterocycles (Figure 6). Group A contains five 2,6-dichloro-3-EDG-pyridine / pyrazine substrates (Figure 6A). The C₂ and C₆ sites have similar ESP values and therefore similar electronic characteristics; however, these sites are distinguished by their local contributions to the LUMO. The C₂ site has the correct LUMO properties (symmetry and coefficients) for favorable oxidative addition via nucleophilic displacement. The C₆ site has a LUMO symmetry-mismatch for nucleophilic displacement and/or low C₆ LUMO contribution, disfavoring oxidative addition to L₂Pd(o). Once again, the observed selectivities match these qualitative predictions: C₂ is the major reactive site in all cases. Product ratios and regiochemistry for these oxidative addition complexes were established by NMR spectroscopic characterization. Single crystal X-ray diffraction further confirmed the assigned structures (4 of the 5 examples), none of which have directing group coordination in the solid-state.

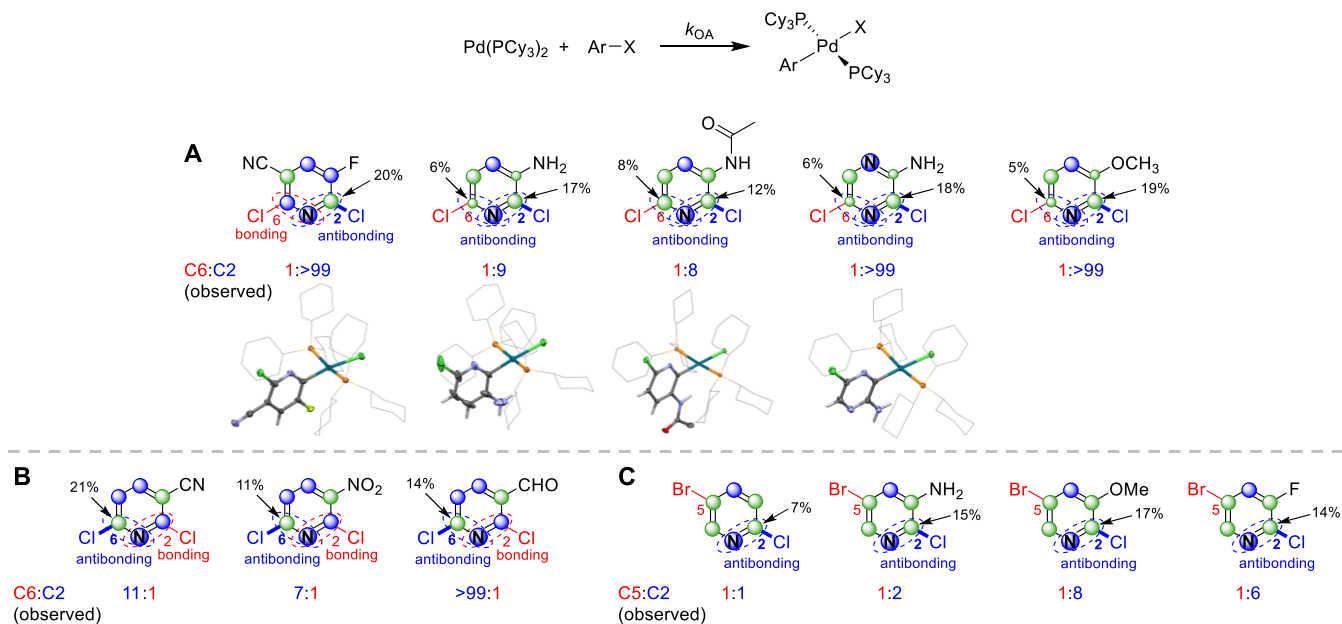


Figure 6. Site-selectivity in oxidative addition of multihalogenated heterocycles to $\text{Pd}(\text{PCy}_3)_2$. A) *LUMO* schematics and product ratios for 2,6-dichloro-3-EDG-pyridines/pyrazine, with solid-state molecular structure (via X-ray crystallography) confirming regiochemistry of the major product (thermal ellipsoids plotted at 50% probability, cyclohexyl groups plotted as wireframe with no hydrogen atoms for clarity). B) *LUMO* schematics and product ratios for 2,6-dichloro-3-EWG-pyridines. C) *LUMO* schematics and product ratios for 2-chloro-5-bromo-3-EDG-pyridines.

In contrast, the three substrates of Group B are 2,6-dichloro-3-EWG-pyridines, which exhibit opposite site-selectivity (EWG = electron-withdrawing group). The presence of the EWG leads to C_6 having a large *LUMO* contribution and being symmetry-matched ($\text{C}_6=\text{N}$ π -antibonding) for nucleophilic displacement, whereas C_2 is symmetry-mismatched ($\text{C}_2=\text{N}$ π -bonding). The observed selectivities agree with this qualitative FMO-based prediction: C_6 is the major site in all three cases, despite the potential for coordination directing oxidative addition to C_2 . Product ratios and regiochemistry were established by NMR spectroscopy.

Finally, we assessed substituted pyridines with different halogens in Group C. These four 2-chloro-5-bromo-3-EDG-pyridines reveal how site-selectivity even for mixed halide substrates can be affected by frontier orbital symmetry (Figure 6C). In general, substrates with -Br and -Cl leaving groups react at the Br site, as documented extensively in the literature.^{34–36} Select cases where C–Cl is the major reactive site are also reported; however, inverting the selectivity to favour Cl often requires extensive reaction and/or catalyst development.³⁷ Here, we sought to determine whether substituent effects alone could make the unconventional C–Cl the favoured site.

For 2-chloro-5-bromopyridine, which has no additional substituents, the *LUMO* coefficient at C_2 is 7%. We previously observed no preference between the two sites in oxidative addition to $\text{Pd}(\text{PCy}_3)_2$ ($\text{C}_2/\text{C}_5=1:1$).³⁶ Adding an EDG at the C_3 position leads to an increase in the *LUMO* contribution at C_2 to 14% ~ 17%. This is qualitatively correlated

with increased C_2 selectivity in oxidative addition to $\text{Pd}(\text{PCy}_3)_2$, from a moderate C_2/C_5 selectivity of 2:1 for the 3- NH_2 derivative, to good C_2/C_5 selectivities of 6:1 for the 3-F derivative and 8:1 for the 3-OMe derivative.

Incorporating FMO features into quantitative oxidative addition reactivity models. Given the observed qualitative correlation between *LUMO* characteristics – symmetry and coefficients – and oxidative addition site-selectivity with $\text{L}_2\text{Pd}(0)$, we returned to our initial quantitative model outliers. Focusing on 2-halopyridines, we investigated if incorporating quantitative FMO descriptors alongside the four descriptors from the initial model (Figure 1) would lead to improved prediction accuracy, especially where strongly electron-donating or withdrawing groups are present.

One such FMO descriptor is the % contribution to the *LUMO* at the reactive carbon center ($\%lumo(\text{C})$), with larger values hypothesized to reduce the predicted $\Delta G^\ddagger_{\text{OA}}$. To account for participation by the neighboring nitrogen in the nucleophilic displacement transition state, we also included its % contribution to the *LUMO* ($\%lumo(\text{N})$). Finally, to account for the importance of relative orbital phase at these two atoms, we established a sign convention for these two *LUMO* descriptors: $\%lumo(\text{C})$ is defined as positive, whereas the $\%lumo(\text{N})$ is either positive (in-phase, bonding) or negative (out-of-phase, antibonding).

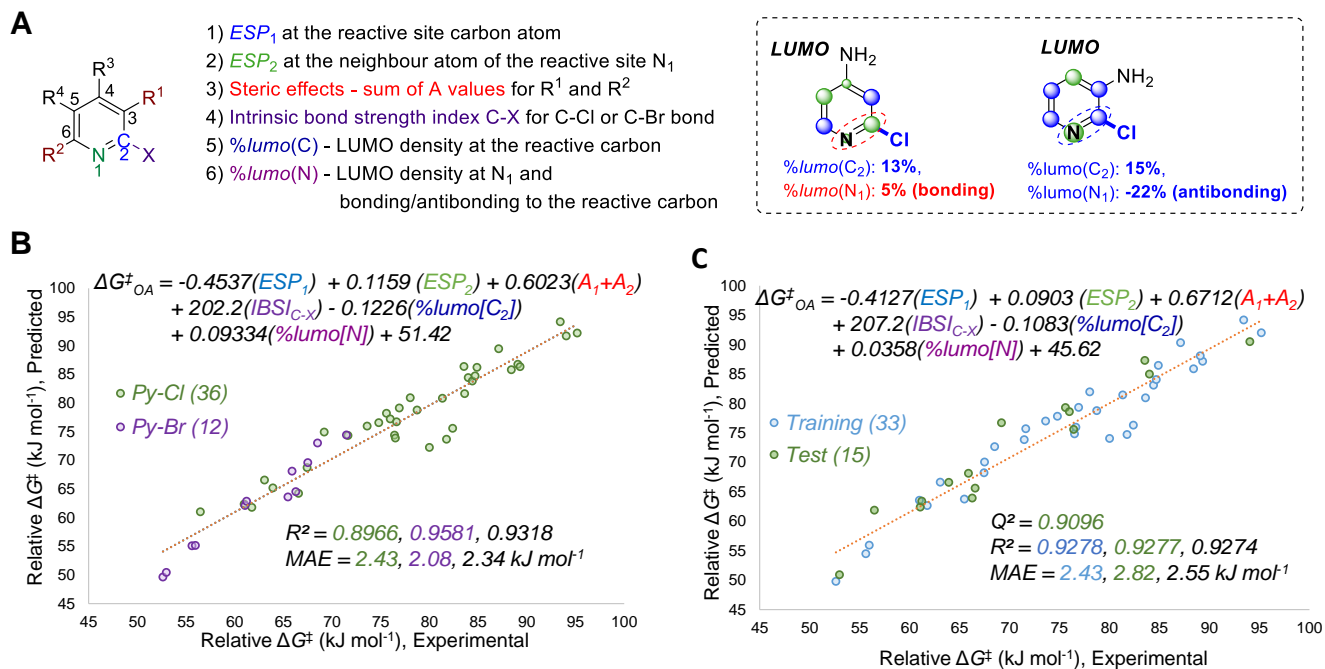


Figure 7. A) Molecular descriptors used to model oxidative addition reactivity as a function of substrate structure for 2-halopyridines; examples of the *LUMO*-based descriptors for bonding (2-chloro-4-aminopyridine) and antibonding (2-chloro-3-aminopyridine) symmetries through the C=N bond. B) Multivariate linear regression model of ΔG^{\ddagger}_{OA} for 48 2-bromo/chloro-pyridines in THF. C) Representative multivariate linear regression model generated using a 70/30 training/test split.

We used a subset of our previously collected oxidative addition dataset,³⁶ containing 48 2-chloro/bromo-pyridine derivatives, to evaluate multivariate linear models containing the additional two *LUMO* descriptors (Figure 7). The resulting model has excellent correlation between the descriptors and the observed ΔG^{\ddagger}_{OA} values, based on the R^2 (0.93) and mean absolute error (MAE = 2.3 kJ mol⁻¹) (Figure 7B). We also evaluated the robustness of this linear model by regression analysis of five random 70/30 training/test splits, with one example shown in Figure 7C.⁴⁸

The resulting linear model is consistent with the hypothesized influence of each descriptor on the predicted ΔG^{\ddagger}_{OA} values. The signs of the coefficients for the two *LUMO* descriptors are as expected: the negative coefficient of $\%lumo(C)$ indicates that a higher *LUMO* contribution from the reactive carbon leads to a faster reaction (*i.e.* smaller ΔG^{\ddagger}_{OA}), while the positive coefficient in front of $\%lumo(N)$ indicates that both a higher *LUMO* contribution and antibonding symmetry at the C=N bond leads to a faster reaction (*i.e.* smaller ΔG^{\ddagger}_{OA}).

The coefficients for the linear equations in Figure 7 are not normalized, which enables direct use of calculated descriptors in the given equations to obtain predicted ΔG^{\ddagger}_{OA} values; however, we did apply min/max normalization to determine the relative contributions of each descriptor to the model.⁴⁸ As for the initial model, the outcome is dominated by the *ESP* values, which account for 65% of the calculated ΔG^{\ddagger}_{OA} . The bond strength descriptor *IBSI* accounts for 21%, and the steric descriptor *A* values account for 7%. Notably, contributions from the *LUMO* descriptors are

small, with only 3% from $\%lumo(C)$, and 4% from $\%lumo(N)$. While this initially appears inconsequential, the energy differences under study are also relatively small (5-10 kJ mol⁻¹) compared to the energy range of the model (50 kJ mol⁻¹). Thus, we view the *LUMO* descriptors as a perturbation of the initial model to account for the more subtle effects imparted by substituent regiochemistry.

Table 1. Comparison of predicted $\Delta\Delta G^{\ddagger}_{OA}$ values without (Fig. 1) or with (Fig. 7) *LUMO* descriptors to experimental values for oxidative addition of 2-chloropyridines.

Entry	EDG	$\Delta\Delta G^{\ddagger}_{OA}$ (kJ mol ⁻¹) ^a		
		Pred. (Fig. 1)	Pred. (Fig. 7)	Exp.
1	NH ₂	3.4	5.8	11.6
2	OMe	2.6	4.9	10.4
3	F	-0.3	1.3	10.8

$$^a \Delta\Delta G^{\ddagger}_{OA} = \Delta\Delta G^{\ddagger}_{OA} (5\text{-EDG}) - \Delta\Delta G^{\ddagger}_{OA} (3\text{-EDG})$$

To assess the model from Figure 7 with specific relevant examples, we compared its ΔG^{\ddagger}_{OA} prediction accuracy against the original model for the three 2-chloro-3/5-EDG-pyridine pairs from Figure 1. The results shown in Table 1

Table 2. Comparison of predicted $\Delta\Delta G^{\ddagger}_{\text{OA}}$ values without (Fig. 1) or with (Fig. 7) inclusion of *LUMO* descriptors and experimental values for oxidative addition of substituted 2,6-dichloro-pyridines/pyridazine.

Entry	Substrate	Major Site	$\Delta\Delta G^{\ddagger}_{\text{OA}}$ (kJ mol ⁻¹) ^a		
			Pred. (Fig. 1)	Pred. (Fig. 7)	Experimental
1		C2	0.4	4.2	>11.5 (>99:1)
2		C2	3.3	5.8	5.5 (9:1)
3		C2	1.8	3.5	5.2 (8:1)
4		C2	8.8	11.8	>11.5 (>99:1)
5		C2	6.8	9.5	>11.5 (>99:1)
6		C6	0.0	3.2	6.0 (11:1)
7		C6	3.4	4.0	4.9 (7:1)
8		C6	6.8	8.1	>11.5 (>99:1)

$$^a\Delta\Delta G^{\ddagger}_{\text{OA}} = \Delta\Delta G^{\ddagger}_{\text{OA}} (\text{minor site}) - \Delta\Delta G^{\ddagger}_{\text{OA}} (\text{major site})$$

reveal a consistent shift toward a larger $\Delta G^{\ddagger}_{\text{OA}}$ gap between the 3-EDG and 5-EDG substrates for the new model, which is more consistent with experiment; however, the *LUMO*-containing model still underestimates the $\Delta\Delta G^{\ddagger}_{\text{OA}}$ by 5.5–9.5 kJ mol⁻¹. For example, the model from Figure 7 predicts a >10:1 difference in relative rates between 3-NH₂ and 5-NH₂ substrates at room temperature, whereas the experimental value is nearly 100:1 (entry 1).

More important from a practical synthetic perspective is model performance for site-selectivity predictions. We applied both models to predict product ratios for the eight 2,6-dichloropyridine derivatives from Figure 6A and B (Table 2). For the five substrates containing electron-donating groups, the initial model significantly underestimates selectivity for the preferred C₂ site (entries 1–5). This is especially true for the 3-fluoro-5-cyano derivative (entry 1), where the predicted ratio is effectively 1:1. In each case, the revised model from Figure 7 improves the predicted

$\Delta\Delta G^{\ddagger}_{\text{OA}}$ by ~2–4 kJ mol⁻¹. For the three electron-deficient 2,6-dichloro-pyridines (entries 6–8), the initial model again significantly underestimates selectivity toward C₆ as the major site, especially for the 3-cyano derivative (entry 6). The revised model improves the predicted $\Delta\Delta G^{\ddagger}_{\text{OA}}$ by 1.5–3 kJ mol⁻¹. While the refined predictions are still systematically underestimated, they are uniformly more useful for synthesis planning than those from the initial model.

To further validate the refined model, particularly in catalytic applications, we examined three reported site-selective cross-coupling reactions involving 2,6-dihalopyridine derivatives (Figure 8). Case A is a site-selective Stille coupling from the work of Nakamura and coworkers, who reported that equimolar stannane and 3,5-dibromopyridine under the given reaction condition yielded mostly the C₃ mono-substituted pyridazine.²⁷ Our previous, *ESP*-focused prediction model³⁶ is qualitatively consistent with the major site; however, it gives only a 6:1 predicted selectivity at

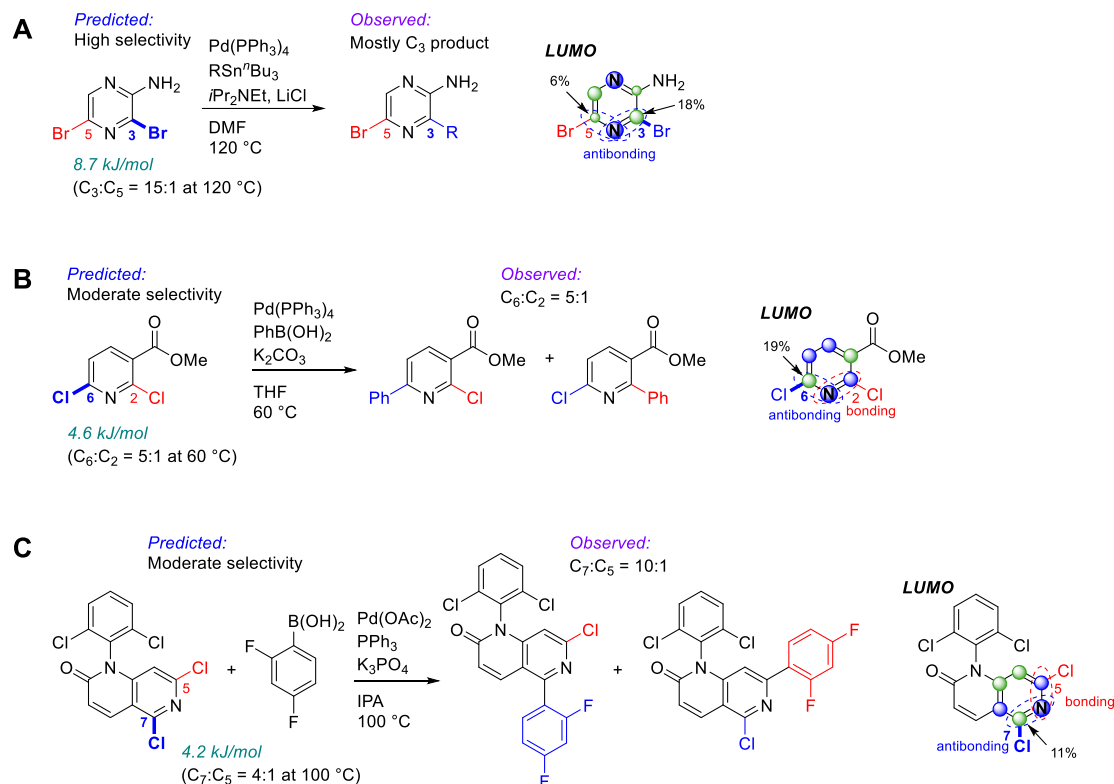


Figure 8. Quantitative selectivity predictions for Pd-catalyzed coupling reactions reported with dihalogenated heterocycles. Colored labels on the heterocycles correspond to predicted major site (blue) and minor site (red). The magnitude of the predicted $\Delta\Delta G_{\text{OA}}^\ddagger$ is given in green. Experimental data from: **A)** Ref. 27; **B)** Ref. 35; **C)** Ref. 49.

120 °C ($\Delta\Delta G_{\text{OA}}^\ddagger = 5.8 \text{ kJ mol}^{-1}$). The *LUMO* of this substrate has significantly more contribution from C₃ than C₅, due to a node passing roughly through the C₂-C₅ plane. This qualitatively points to C₃ as the expected major site, consistent with experiment. Using the FMO-containing model from Figure 7 gives a quantitative selectivity prediction of 15:1 at 120 °C, which is more consistent with the observed high selectivity than our prior model.

Case B involves a Pd(PPh₃)₄-catalyzed Suzuki-Miyaura coupling with methyl 2,6-dichloronicotinate, and is reported to give C₆ arylation as the major product (5:1 ratio).³⁵ Our prior model is again only qualitatively consistent, predicting C₆ as the major site, but with only a 2.5:1 ratio at 60 °C. Based on the *LUMO* symmetry, C₆ is expected to be favored. Quantitatively, the revised model predicts 5:1 (C₆:C₂) selectivity at 60 °C, again showing an improvement by including FMO descriptors.

In Case C, we examined the Suzuki-Miyaura coupling a dichloro-naphthyridone substrate, which is an intermediate toward an investigational MAP kinase inhibitor.⁴⁹ This reaction proceeds with a product ratio of ~10:1 favoring arylation at C₇ when PPh₃ is used as the ligand. The *LUMO* symmetry is consistent with this selectivity, based on C₇=N being π -antibonding and C₅=N being π -bonding. The revised model predicts a 4:1 selectivity favoring C₇ at 100 °C, compared to a 2.8:1 ratio predicted by the previous model.

Finally, the revised model is not without limitations. Specifically, applying it to predict site-selectivity for the 2-

Cl-5-Br-pyridines in Figure 6C led to poor quantitative agreement with experiment.⁴⁸ This is undoubtedly due to a limitation of the source data for the revised model, which is focused on 2-halopyridines. Further work is underway to improve the scope and accuracy of these oxidative addition models by expanding our datasets to better represent FMO-based effects with a variety of substitution patterns.

CONCLUSIONS

In summary, we have established how substituent effects on frontier molecular orbital symmetry affect the rate/selectivity of oxidative addition for halopyridines and related heterocycles. With 14-electron L₂Pd(0) complexes, exemplified by Pd(PCy₃)₂, coordination by directing groups is not necessary to explain the observed reactivity. Instead, substrate *LUMO* symmetry dictates whether a nucleophilic displacement mechanism or 3-centered mechanism operates, based on symmetry matching to the π -symmetry *HOMO* of the bent L-Pd-L unit. The faster oxidative addition rates of 2-chloro-3-EDG-pyridines compared to their 5-EDG analogues is correlated to high *LUMO* contribution at C₂ and antibonding symmetry through the C=N bond for the former regioisomers. Both of these features favor the lower activation energy nucleophilic substitution mechanism. In contrast, the 5-EDG regioisomers have *LUMO* symmetries containing a node through the C₅-C₂ plane, making the *LUMO* contribution at C₂ minimal. Instead, the higher energy *LUMO*+1 is the relevant FMO, and

DFT calculations reveal these substrates proceed through a 3-centered oxidative addition mechanism.

These insights can be extended to other substitution patterns, including with electron-withdrawing groups, enabling qualitative predictions for relative rate / site-selectivity of oxidative addition to $L_2Pd(o)$ species. We confirmed these predictions experimentally by isolating and characterizing oxidative addition complexes of 2,6-dichloropyridines with 3-EDG and 3-EWG substituents. Furthermore, 3-EDG substituents on 2-chloro-5-bromopyridines lead to the 2-Cl site being favored for oxidative addition, contrary to the intrinsic site-selectivity. We also further generalized these *LUMO*-based features to refine our prior quantitative model for site selectivity, which does result in improved performance for predicting site-selectivity in substituted 2,6-dihalopyridines and related heterocycles.

Finally, this work demonstrates how studying outliers to quantitative structure-reactivity relationships can reveal mechanistic changes and nuances that are otherwise difficult to identify. As more large datasets and predictive models are reported for a variety of reaction classes, important mechanistic insights will likely result from interrogating systematic outliers. Not only will this enable improved mechanism-based models and predictions, but also expand our understanding of the structure-mechanism landscape in organic chemistry.

ASSOCIATED CONTENT

Supporting Information. Detailed experimental procedures and computational methods, characterization data for oxidative addition complexes and regioisomer mixtures, tables of molecular descriptors, and additional regression plots (PDF format); data files containing extended tables of descriptors and regression analysis (*xlsx* format), and Cartesian coordinate files for calculated structures and transition states (*xyz* format). CIFs for Pd oxidative addition complexes are deposited with the CCDC with deposition numbers CCDC 2334080-2334084.

AUTHOR INFORMATION

Corresponding Authors

* Irina Paci – Department of Chemistry, University of Victoria, Victoria, British Columbia V8P 5C2, Canada;
orcid.org/0000-0002-8726-3318; Email: ipaci@uvic.ca

* David C. Leitch – Department of Chemistry, University of Victoria, Victoria, British Columbia V8P 5C2, Canada;
orcid.org/0000-0002-8726-3318; Email: dcleitch@uvic.ca

Author Contributions

The manuscript was written through contributions of all authors. All authors have given approval to the final version of the manuscript.

Notes

The authors declare no competing financial interests.

ACKNOWLEDGMENTS

We acknowledge and respect the Lekwungen peoples on whose traditional territory the University of Victoria (UVic) stands, and the Songhees, Esquimalt and WSÁNEĆ peoples whose historical relationships with the land continue to this day. We also acknowledge funding from the New Frontiers in Research Fund – Exploration and the NSERC Discovery Grant programs. D.C.L. thanks the Research Corporation for Science Advancement for a Cottrell Scholar Award.

REFERENCES

- (1) Magano, J.; Dunetz, J. R. Large-Scale Applications of Transition Metal-Catalyzed Couplings for the Synthesis of Pharmaceuticals. *Chem. Rev.* **2011**, *111*, 2177–2250. <https://doi.org/10.1021/cr100346g>.
- (2) Campeau, L.-C.; Hazari, N. Cross-Coupling and Related Reactions: Connecting Past Success to the Development of New Reactions for the Future. *Organometallics* **2019**, *38*, 3–35. <https://doi.org/10.1021/acs.organomet.8b00720>.
- (3) a) Reeves, E. K.; Entz, E. D.; Neufeldt, S. R. Chemodivergence between Electrophiles in Cross-Coupling Reactions. *Chem. Eur. J.* **2021**, *27*, 6161–6177. <https://doi.org/10.1002/chem.202004437>. b) Rio, J.; Liang, H.; Perrin, M.-E. L.; Perego, L. A.; Grimaud, L.; Payard, P.-A. We Already Know Everything about Oxidative Addition to Pd(o): Do We? *ACS Catal.* **2023**, *13*, 11399–11421.
- (4) Stille, J. K.; Lau, K. S. Y. Mechanisms of Oxidative Addition of Organic Halides to Group 8 Transition-Metal Complexes. *Acc. Chem. Res.* **1977**, *10*, 434–442. <https://doi.org/10.1021/ar50120a002>.
- (5) Portnoy, M.; Milstein, D. Mechanism of Aryl Chloride Oxidative Addition to Chelated Palladium(o) Complexes. *Organometallics* **1993**, *12*, 1665–1673. <https://doi.org/10.1021/om00029a026>.
- (6) Amatore, C.; Jutand, A.; Khalil, F.; M'Barki, M. A.; Motier, L. Rates and Mechanisms of Oxidative Addition to Zerovalent Palladium Complexes Generated in Situ from Mixtures of Pd⁰(dba)₂ and Triphenylphosphine. *Organometallics* **1993**, *12*, 3168–3178. <https://doi.org/10.1021/om00032a045>.
- (7) Jutand, A.; Mosleh, A. Rate and Mechanism of Oxidative Addition of Aryl Triflates to Zerovalent Palladium Complexes. Evidence for the Formation of Cationic (σ-Aryl)Palladium Complexes. *Organometallics* **1995**, *14*, 1810–1817. <https://doi.org/10.1021/om00004a038>.
- (8) Gooßen, L. J.; Koley, D.; Hermann, H.; Thiel, W. The Mechanism of the Oxidative Addition of Aryl Halides to Pd-Catalysts: A DFT Investigation. *Chem. Commun.* **2004**, 2141–2143. <https://doi.org/10.1039/B409144B>.
- (9) Senn, H. M.; Ziegler, T. Oxidative Addition of Aryl Halides to Palladium(o) Complexes: A Density-Functional Study Including Solvation. *Organometallics* **2004**, *23*, 2980–2988. <https://doi.org/10.1021/om049963n>.
- (10) Ahlquist, M.; Norrby, P.-O. Oxidative Addition of Aryl Chlorides to Monoligated Palladium(o): A DFT-SCRF Study. *Organometallics* **2007**, *26*, 550–553. <https://doi.org/10.1021/om0604932>.
- (11) Barrios-Landeros, F.; Carrow, B. P.; Hartwig, J. F. Effect of Ligand Steric Properties and Halide Identity on the Mechanism for Oxidative Addition of Haloarenes to Trialkylphosphine Pd(o) Complexes. *J. Am. Chem. Soc.* **2009**, *131*, 8141–8154. <https://doi.org/10.1021/ja900798s>.

- (12) McMullin, C. L.; Jover, J.; Harvey, J. N.; Fey, N. Accurate Modelling of Pd(o) + PhX Oxidative Addition Kinetics. *Dalton Trans.* **2010**, *39*, 10833–10836. <https://doi.org/10.1039/C0DT00778A>.
- (13) a) Besora, M.; Maseras, F. The Diverse Mechanisms for the Oxidative Addition of C–Br Bonds to Pd(PR₃) and Pd(PR₃)₂ Complexes. *Dalton Trans.* **2019**, *48*, 16242–16248. <https://doi.org/10.1039/C9DT03155C>. b)
- (14) Maes, B. U. W.; Verbeeck, S.; Verhelst, T.; Ekomié, A.; von Wolff, N.; Lefèvre, G.; Mitchell, E. A.; Jutand, A. Oxidative Addition of Haloheteroarenes to Palladium(o): Concerted versus SNAr-Type Mechanism. *Chem. Eur. J.* **2015**, *21*, 7858–7865. <https://doi.org/10.1002/chem.201406210>.
- (15) Norman, J. P.; Larson, N. G.; Neufeldt, S. R. Different Oxidative Addition Mechanisms for 12- and 14-Electron Palladium(o) Explain Ligand-Controlled Divergent Site Selectivity. *ACS Catal.* **2022**, *12*, 8822–8828. <https://doi.org/10.1021/acscatal.2c01698>.
- (16) Legault, C. Y.; Garcia, Y.; Merlic, C. A.; Houk, K. N. Origin of Regioselectivity in Palladium-Catalyzed Cross-Coupling Reactions of Polyhalogenated Heterocycles. *J. Am. Chem. Soc.* **2007**, *129*, 12664–12665. <https://doi.org/10.1021/ja0757850>.
- (17) Schoenebeck, F.; Houk, K. N. Ligand-Controlled Regioselectivity in Palladium-Catalyzed Cross Coupling Reactions. *J. Am. Chem. Soc.* **2010**, *132*, 2496–2497. <https://doi.org/10.1021/ja9077528>.
- (18) Almond-Thynne, J.; C. Blakemore, D.; C. Pryde, D.; C. Spivey, A. Site-Selective Suzuki–Miyaura Coupling of Heteroaryl Halides – Understanding the Trends for Pharmaceutically Important Classes. *Chem. Sci.* **2017**, *8*, 40–62. <https://doi.org/10.1039/C6SC02188B>.
- (19) Palani, V.; Hugelshofer, C. L.; Kevlishvili, I.; Liu, P.; Sarpong, R. A Short Synthesis of Delavatine A Unveils New Insights into Site-Selective Cross-Coupling of 3,5-Dibromo-2-Pyrrone. *J. Am. Chem. Soc.* **2019**, *141*, 2652–2660. <https://doi.org/10.1021/jacs.8b13012>.
- (20) Palani, V.; Perea, M. A.; Sarpong, R. Site-Selective Cross-Coupling of Polyhalogenated Arenes and Heteroarenes with Identical Halogen Groups. *Chem. Rev.* **2022**, *122*, 10126–10169. <https://doi.org/10.1021/acs.chemrev.1c00513>.
- (21) Norman, J. P.; Larson, N. G.; Entz, E. D.; Neufeldt, S. R. Unconventional Site Selectivity in Palladium-Catalyzed Cross-Couplings of Dichloroheteroarenes under Ligand-Controlled and Ligand-Free Systems. *J. Org. Chem.* **2022**, *87*, 7414–7421. <https://doi.org/10.1021/acs.joc.2c00665>.
- (22) Elias, E. K.; Rehbein, S. M.; Neufeldt, S. R. Solvent Coordination to Palladium Can Invert the Selectivity of Oxidative Addition. *Chem. Sci.* **2022**, *13*, 1618–1628. <https://doi.org/10.1039/D1SC05862B>.
- (23) Ibsen, G. M.; Menezes da Silva, V. H.; Pettigrew, J. C.; Neufeldt, S. R. Triflate-Selective Suzuki Cross-Coupling of Chloro- and Bromoaryl Triflates Under Ligand-Free Conditions. *Chem. Asian J.* **2023**, *18*, e202300036. <https://doi.org/10.1002/asia.202300036>.
- (24) Engle, K. M.; Mei, T.-S.; Wasa, M.; Yu, J.-Q. Weak Coordination as a Powerful Means for Developing Broadly Useful C–H Functionalization Reactions. *Acc. Chem. Res.* **2012**, *45*, 788–802. <https://doi.org/10.1021/ar200185g>.
- (25) Sambiagio, C.; Schönbauer, D.; Blicke, R.; Dao-Huy, T.; Pototschnig, G.; Schaaf, P.; Wiesinger, T.; Zia, M. F.; Wencel-Delord, J.; Besset, T.; Maes, B. U. W.; Schnürch, M. A Comprehensive Overview of Directing Groups Applied in Metal-Catalysed C–H Functionalisation Chemistry. *Chem. Soc. Rev.* **2018**, *47*, 6603–6743. <https://doi.org/10.1039/C8CS00201K>.
- (26) Mandal, R.; Garai, B.; Sundararaju, B. Weak-Coordination in C–H Bond Functionalizations Catalyzed by 3d Metals. *ACS Catal.* **2022**, *12*, 3452–3506. <https://doi.org/10.1021/acscatal.1c05267>.
- (27) Nakamura, H.; Takeuchi, D.; Murai, A. Synthesis of 5- and 3,5-Substituted 2-Aminopyrazines by Pd Mediated Stille Coupling. *Synlett* **1995**, 1227–1228. <https://doi.org/10.1055/s-1995-5249>.
- (28) Hikawa, H.; Yokoyama, Y. Cross-Coupling Reaction on N-(3,5-Dibromo-2-Pyridyl)Piperazines: Regioselective Synthesis of 3,5-Disubstituted Pyridylpiperazines. *Tetrahedron* **2010**, *66*, 9552–9559. <https://doi.org/10.1016/j.tet.2010.09.100>.
- (29) Hilton, S.; Naud, S.; Caldwell, J. J.; Boxall, K.; Burns, S.; Anderson, V. E.; Antoni, L.; Allen, C. E.; Pearl, L. H.; Oliver, A. W.; Wynne Aherne, G.; Garrett, M. D.; Collins, I. Identification and Characterisation of 2-Aminopyridine Inhibitors of Checkpoint Kinase 2. *Bioorg. Med. Chem.* **2010**, *18*, 707–718. <https://doi.org/10.1016/j.bmc.2009.11.058>.
- (30) Blaise, E.; Kümmerle, A. E.; Hammoud, H.; de Araújo-Júnior, J. X.; Bihel, F.; Bourguignon, J.-J.; Schmitt, M. Access to 4-Alkylaminopyridazine Derivatives via Nitrogen-Assisted Regioselective Pd-Catalyzed Reactions. *J. Org. Chem.* **2014**, *79*, 10311–10322. <https://doi.org/10.1021/jo501930s>.
- (31) Yang, C.-G.; Liu, G.; Jiang, B. Preparing Functional Bis(Indole) Pyrazine by Stepwise Cross-Coupling Reactions: An Efficient Method to Construct the Skeleton of Dragmacidin D. *J. Org. Chem.* **2002**, *67*, 9392–9396. <https://doi.org/10.1021/jo026450m>.
- (32) Niemeyer, Z. L.; Milo, A.; Hickey, D. P.; Sigman, M. S. Parameterization of Phosphine Ligands Reveals Mechanistic Pathways and Predicts Reaction Outcomes. *Nature Chem.* **2016**, *8*, 610–617. <https://doi.org/10.1038/nchem.2501>.
- (33) Newman-Stonebraker, S. H.; Smith, S. R.; Borowski, J. E.; Peters, E.; Gensch, T.; Johnson, H. C.; Sigman, M. S.; Doyle, A. G. Univariate Classification of Phosphine Ligation State and Reactivity in Cross-Coupling Catalysis. *Science* **2021**, *374*, 301–308. <https://doi.org/10.1126/science.abj4213>.
- (34) Houpis, I. N.; Huang, C.; Nettekoven, U.; Chen, J. G.; Liu, R.; Canters, M. Carboxylate Directed Cross-Coupling Reactions in the Synthesis of Trisubstituted Benzoic Acids. *Org. Lett.* **2008**, *10*, 5601–5604. <https://doi.org/10.1021/ol802349u>.
- (35) Yang, W.; Wang, Y.; Corte, J. R. Efficient Synthesis of 2-Aryl-6-Chloronicotinamides via PXPd₂-Catalyzed Regioselective Suzuki Coupling. *Org. Lett.* **2003**, *5*, 3131–3134. <https://doi.org/10.1021/ol035188g>.
- (36) Lu, J.; Donnecke, S.; Paci, I.; Leitch, D. C. A Reactivity Model for Oxidative Addition to Palladium Enables Quantitative Predictions for Catalytic Cross-Coupling Reactions. *Chem. Sci.* **2022**, *13*, 3477–3488. <https://doi.org/10.1039/D2SC00174H>.
- (37) Suresh, C. H.; Alexander, P.; Vijayalakshmi, K. P.; Sajith, P. K.; Gadre, S. R. Use of Molecular Electrostatic Potential for Quantitative Assessment of Inductive Effect. *Phys. Chem. Chem. Phys.* **2008**, *10*, 6492–6499. <https://doi.org/10.1039/B809561B>.
- (38) Sayyed, F. B.; Suresh, C. H. Quantification of Substituent Effects Using Molecular Electrostatic Potentials: Additive Nature and Proximity Effects. *New J. Chem.* **2009**, *33*, 2465–2471. <https://doi.org/10.1039/B9NJ00333A>.
- (39) Remya, G. S.; Suresh, C. H. Quantification and Classification of Substituent Effects in Organic Chemistry: A Theoretical Molecular Electrostatic Potential Study. *Phys. Chem. Chem. Phys.* **2016**, *18*, 20615–20626. <https://doi.org/10.1039/C6CP02936A>.
- (40) Anjali, B. A.; Suresh, C. H. Interpreting Oxidative Addition of Ph–X (X = CH₃, F, Cl, and Br) to Monoligated Pd(o) Catalysts Using Molecular Electrostatic Potential. *ACS Omega* **2017**, *2*, 4196–4206. <https://doi.org/10.1021/acsomega.7b00745>.
- (41) Gadre, S. R.; Suresh, C. H.; Mohan, N. Electrostatic Potential Topology for Probing Molecular Structure, Bonding and

Reactivity. *Molecules* **2021**, *26*, 3289. <https://doi.org/10.3390/molecules26113289>.

(42) Hirsch, J. A. Table of Conformational Energies—1967. In *Topics in Stereochemistry*; John Wiley & Sons, Ltd, 1967; pp 199–222. <https://doi.org/10.1002/9780470147108.ch4>.

(43) Klein, J.; Khartabil, H.; Boisson, J.-C.; Contreras-García, J.; Piquemal, J.-P.; Hénon, E. New Way for Probing Bond Strength. *J. Phys. Chem. A* **2020**, *124*, 1850–1860. <https://doi.org/10.1021/acs.jpca.9b09845>.

(44) Lu, J.; Paci, I.; Leitch, D. C. A Broadly Applicable Quantitative Relative Reactivity Model for Nucleophilic Aromatic Substitution (S_NAr) Using Simple Descriptors. *Chem. Sci.* **2022**, *13*, 12681–12695. <https://doi.org/10.1039/D2SC04041G>.

(45) Note that $Pd(PCy_3)_2$ is also reported to undergo oxidative addition to bromobenzene via the monoligated $Pd(PCy_3)$ species. Based on results from Neufeldt and co-workers, this species should favor a 3-centered mechanism (refs. 15 and 46).

Mitchell, E. A.; Jessop, P. G.; Baird, M. C. A Kinetics Study of the Oxidative Addition of Bromobenzene to $Pd(PCy_3)_2$ (Cy = Cyclohexyl) in a Nonpolar Medium: The Influence on Rates of Added PCy_3 and Bromide Ion. *Organometallics* **2009**, *28*, 6732–6738. <https://doi.org/10.1021/om900679w>.

(46) Kania, M. J.; Reyes, A.; Neufeldt, S. R. Oxidative Addition of (Hetero)Aryl (Pseudo)Halides at Palladium(o): Origin and Significance of Divergent Mechanisms. *ChemRxiv* **2024**.

(47) Wolters, L. P.; Bickelhaupt, F. M. Nonlinear d^{10} - ML_2 Transition-Metal Complexes. *ChemistryOpen* **2013**, *2*, 106–114. <https://doi.org/10.1002/open.201300009>.

(48) See Supporting Information for More Details.

(49) Chung, J. Y. L.; Cai, C.; McWilliams, J. C.; Reamer, R. A.; Dormer, P. G.; Cvetovich, R. J. Efficient Synthesis of a Trisubstituted 1,6-Naphthyridone from Acetonedicarboxylate and Regioselective Suzuki Arylation. *J. Org. Chem.* **2005**, *70*, 10342–10347. <https://doi.org/10.1021/jo0514927>.